RANS Simulation of Laminar-Turbulent Transition in Separation Bubbles on Airfoils

Jean Perraud[1], Luis Bernardos[2], Julien Marty[2], Gregory Delattre[1]
1 - ONERA/DMPE, Université de Toulouse - F-31055 Toulouse - FRANCE
2 – ONERA/DAAA, Université Paris-Saclay - F-92190 Meudon – FRANCE
Jean.perraud@onera.fr

ABSTRACT

Predicting the location of laminar-turbulent transition, and modelling the transition region inside a separation bubble are two related questions presently limiting the performance of flow simulations. Considering these questions requires both an understanding of the underlying physics and a number of improvements of the available numerical tools. Several airfoils presenting short and long laminar bubbles are considered, trying to define a common approach with an internal prediction of laminar-turbulent transition. Comparisons to existing measurements and current predictions will be presented. Two methods for transition prediction are used with the same elsA numerical platform, transition criteria and the $\gamma - \overline{R_{\theta_T}}$ *approach.*

NOMENCLATURE

C_p : Pressure coefficient
C_f : Skin friction coefficient
Hi : Incompressible shape factor($\frac{\delta_{1i}}{\theta_i}$)
k : Turbulent kinetic energy
k_L : Laminar kinetic energy
M : Mach number
N : N-factor, perturbations amplification
Re_L : Reynolds number based on length L
s : Wall tangent curvilinear abscissa
S_{ij} : strain-rate tensor
Tu : Turbulence level ($\frac{1}{U}\sqrt{\frac{2k}{3}}$)
U_∞ : Velocity
y+ : distance in wall units, $\rho u_\tau y/\mu$
Λ_2 : Pohlhausen parameter

θ : Momentum thickness
δ_1 : Displacement thickness
γ : intermittency
μ : molecular dynamic viscosity
μ_t : dynamic eddy viscosity
ν : molecular cinematic viscosity
ω : turbulence specific dissipation rate
Ω_{ij} : rotation-rate tensor
Subscripts :
∞ : at upstream reference location
e : at the boundary layer edge
T : at transition location
i : incompressible
t : turbulent quantity

1.0 INTRODUCTION

Airfoils presenting a laminar separation at low Reynolds numbers, with laminar-turbulent transition in the separation region, are becoming more common with the wide use of unmanned aerial vehicles (UAVs), and micro air vehicles (MAVs). Other cases of interest include propellers, helicopter and turbine blades, transonic Natural Laminar Flow (NLF) wings, as well as low speed high-lift wings at take-off and landing. An accurate prediction of an airfoil performance requires a precise prediction of the separation extent. Being able to predict the limit for a stable re-attachment of the flow is crucial for determining the stall limits of an airfoil.

While methods based on the interacting boundary layer concept are commonly used for low Reynolds number profile design [1], extension to 3D wings and unsteady problems requires the use of Reynolds

Averaged Navier Stokes (RANS) solvers. Also, RANS approaches may be used to compute boundary layer profiles inside the separation bubble, useful for stability analysis and the development of transition prediction criterion. Several approaches for the numerical simulation of detached flows are possible. While Direct Numerical Simulation (DNS) may provide information very difficult to measure inside small separation bubble [2], the simulation cost makes it at present unacceptable for current design work. Large Eddy Simulation (LES) is an intermediate solution, still rather expensive but allowing to simulate the transition dynamics [3],[4]. A number of authors have addressed this problem in the past, either looking at the development of simplified transition prediction methods or the coupling between RANS and stability codes [5]-[10]. Also, the task group AVT-101 conducted an important project [11] in the field, dedicated to low Reynolds number Micro Air Vehicles and ending in 2006.

Computing complex configurations of industrial interest, with strong three-dimensional effects and compressibility is best done using Reynolds Averaged Navier Stokes (RANS) solvers, the preferred approach for design, compatible with present computing capabilities. This also requires a simplified description of the aerodynamic conditions, with upstream perturbations described through a few scalar parameters.

While a number of paths from laminar to turbulent flow are possible, depending on pressure gradient, Reynolds number, and the level of ambient perturbations, in the most common scenario Tollmien Schlichting (TS) instabilities starting to grow upstream of the separation location have been shown to feed Kelvin-Helmholtz (KH) instabilities in the shear layer on the upper region of the separation [12], with a larger growth rate than the initial TS instabilities. Capturing this mechanism with Large Eddy Simulation (LES) was done by a number of authors [13][3] in presence of low upstream perturbations.

Another class of problems, labelled 'internal aerodynamics', deal with turbine blades operating in highly perturbed flows, but still presenting a portion of laminar flow near the leading edge of the blades. Depending on conditions, this laminar region may extend to a large part of the suction side, ending with a transitional separation region. Computing such flows requires a different approach, as classical Tollmien Schlichting instabilities are bypassed by stronger phenomenon. The current preferred method is based on the Menter-Langtry $\gamma - \overline{R_{\theta_T}}$ approach [14] relying on a transition criterion derived from Langtry and Abu-Ghannam and Shaw criteria. This method may generate quite acceptable results but must be used with caution due to the weaknesses of the empirical transition criterion formulated without compressibility term and which was shown to lack precision for the impact of pressure gradient [15]. Note that methods based on the 'laminar kinetic energy' theory and the dynamics of Klebanoff ‘modes’ [16], introducing ω-k_T-k_L models, would be most adapted for these cases, but are not yet fully developed.

Experiments may produce a range of results, depending on the perturbation level. At very low upstream turbulence, an unsteady flow may be observed (open separation). A small increase of turbulence may cause the flow to reattach, resulting in a steady separation. With a large turbulence level, the separation may disappear depending on the pressure gradient and the Reynolds number. Turbine blades show specific pressure gradients and designs prone to present a separation in presence of a large turbulence level. Detailed information inside a laminar separation bubble is difficult to obtain in experiments due to the small size of the bubble. µ-PIV has been developed [17] to improve this point.

A number of questions may appear when considering both external and internal aerodynamics. In the first case, the computational domain extends to about 20 chords around the profile, and boundary conditions are required for the turbulent quantities on the upstream limit. The values imposed on the boundary are seen to decay, mostly due to the natural decay of turbulence but also to numerical artefacts. This was examined in a paper by Spalart and Rumsey [18], who proposed as a solution to impose as boundary conditions the value desired in the vicinity of the profile and blocking any variation below the imposed values using cut-off limits. In the second case, the entrance section is usually placed a few chords upstream of the blade, and in facilities used for studying turbine blades, of limited length, the link between an imposed turbulence level in

the inlet section and that at the leading edge of the blade may be predicted and measured, allowing a more precise description of upstream conditions [19].

In classical transition studies with RANS solvers, the usual practice consists in assuming that the small level of turbulent kinetic energy in the flow is decoupled from the incoming perturbations of whatever nature (acoustics, turbulence, roughness...). As the turbulent quantities are present in the RANS calculation, but kept at a minimal level upstream of transition, that level may indeed be extremely small, being assumed that the turbulence model will cause a rapid rise in turbulent kinetic energy k, past transition. This is fine when the Reynolds number is large enough, although this is not always the case just downstream of a transition point. In fact, it may be observed that this initial level has an impact on the initial production of turbulent kinetic energy.

Hence, two ways of accelerating this initial production are available, either impose an initial level or determine an intermittency function - or a transition function - applied on the production term with values larger than 1 over a short distance.

Methods and results in this paper will first show that a predicted transition location may be computed in course of the RANS calculation, in the separated region. Then, turbulence production will cause a turbulent re-attachment, producing a steady, converged solution for a range of flow conditions. Very similar initial conditions will be used considering four different cases, the profiles SD7003, ONERA-D and T106C, and a flat plate with imposed pressure gradient based on the OA209 profile. This will be obtained using a modified Gleyzes criterion [6].

2.0 SHORT DESCRIPTION OF TEST CASES

A number of airfoils may be considered for this type of work, one question being the availability of experimental results for validation.

The OA209 profile, with or without cyclic variations of incidence, has been considered at ONERA for a number of years [10], [20]. A test case derived from it consists of a flat plate with an upper slip wall which produces a streamwise variable adverse pressure gradient on the lower no-slip wall. The variable adverse pressure gradient induced by the curved upper wall mimics the pressure distribution at the leading-edge region of an OA209 airfoil near stall [21]. The freestream Mach number and chord-based Reynolds number of this airfoil configuration are, respectively, $M_\infty = 0.16$ and $Re_C = 1.8\ 10^6$. The incoming flow is laminar and separates from the no-slip wall as a consequence of the adverse pressure gradient. Downstream of the laminar separation, the flow transitions to turbulence and reattaches to the no-slip wall, forming a transitional bubble. The derived test case was considered by C. Laurent using a DNS approach [32]. While a very refined mesh was used for the DNS (1428x330 pts), several meshes were used for RANS computations with 714x165 to 178x165 pts. A mesh convergence study is reported in [31].

The SD7003 is a low Reynolds number profile designed for sailplane and Micro Air Vehicles [22], which presents a long separation bubble over a range of incidences. It as been considered in a number of published papers [23][24][3] at a chord Reynolds number of 60,000 and was a selected test case in [11]. For the work presented here, two meshes were used. The first comprises 447x101 pts, with 50 pts past the trailing edge and 198 pts on both pressure and suction sides, allowing between 45 and 55 pts in the boundary layer region and a $y+ < 0.1$. The second mesh comprises 867x176 pts with 96 in the wake, 179 on the pressure side and 593 on the suction side, allowing $y+ < 1$ and 80 pts in the boundary layer.

The symmetrical ONERA-D profile has been used for many years as a test bed for transition tools development. Most experiments and test cases assume a triggered transition on the suction side, but without triggering a short separation bubble appears near the leading edge with incidences as low as 1 deg. Wind tunnel experiments on a 2D model with 0.75 m chord were done between 10 and 40 m/s with a turbulence

level of 0.15% in 1969, resulting in pressure distributions measurements and separation length detection. The 40 m/s configuration will be considered in this paper, with a Reynolds number of 1.91 10^6. Experimental data were re-analysed from the initial test report, but there is little information concerning data uncertainties. The mesh for this case contains 878x209 pts, with 101 pts in the wake and 389 on both sides of the profile. Vertical distribution allows to obtain about 50 pts inside the boundary layer. Stability calculations were in the past realised using the boundary layer profiles extracted from the RANS flow, successfully compared against stability results from boundary layers profiles generated using the 3C3D boundary layer code.

For turbine flows, a classical test bed involves the T106C blade in a wide range of flow conditions. This test case is based on the experiments performed by Michalek et al. [25]. They studied the low-pressure high-lift turbine blade T106C on a linear cascade in the VKI S1/C high-speed wind tunnel operating at exit Mach number of M = 0.65. Multiple cases were analysed, particularly for varying chord-based Reynolds number and free-stream turbulence levels. This configuration was studied by both A. Benyahia[38] and A. Minot[19] in their doctoral work. A. Minot describes the mesh used and conducted a mesh convergence study, reported in [19].

2.1 General remarks concerning the simulations

A main source of uncertainty identified from this work is the lack of a precise description of the incoming turbulence in the region of the leading edge of the profiles. In most experiments, only the turbulence intensity is measured at one location upstream of the model. Due to the natural decay of turbulence, the actual level some distance downstream will be lower. This is more pronounced in case of large Tu levels, and may explain some discrepancies between predictions and experiments. On the numerical side, the Mack's law is often used to relate a transition N-factor to the local turbulence level. Even with a laminar region, the flow is computed with a turbulence model which requires boundary values, but with a turbulence level also affected by turbulence decay. One option in our calculations is to define two turbulence levels, one independent from the turbulence model and specifically used to determine the transition location, and the other related to the turbulence model.

Another important remark is that a good precision is required in the computation of the laminar boundary layer, with a well distributed number of points along the boundary layer height. Care must be taken to avoid concentrating too many points in the wall region of the boundary layer. In order to allow a precise computation of the boundary layer parameters, boundary layer profiles must be correctly computed, thus requiring a low dissipation numerical scheme. The results presented here were obtained with either the Roe or a variant of the AUSM+ schemes.

3.0 RANS BASED METHODS WITH COMPUTED TRANSITION

The Airbus/Safran/ONERA elsA software is used in structured blocks, steady RANS mode with well adapted settings allowing a precise enough computation of the boundary layers, which would allow to compute the amplification rate of instabilities in the laminar region. Several turbulence models based on k-ω transport equations have been used.

3.1 Classical Transition Prediction

The laminar or turbulent state of a boundary layer may be characterized using the intermittency function γ, which represents the fraction of time over which the flow is turbulent. While this physical intermittency varies from zero to one, a numerical equivalent may be defined, controlling the level of turbulence production. When using transition criteria, γ is defined at wall points and its value applies to all the points along a normal to the wall direction, up to a maximal distance. γ is then used as a weighting function applied to the eddy viscosity coefficient: $\mu_{eff} = \mu + \gamma\mu_t$. In case of transport equation turbulence models for which the k production term is proportional to μ_t , using $\gamma\mu_t$ prevents the production of turbulence. Another approach involves the introduction of the intermittency into the k equation of the turbulence model, replacing the

production term P_k with γP_k. Furthermore, this numerical intermittency may locally be greater than one, in order to accelerate the turbulence production. This is the case with the function proposed by Arnal [26], which reaches a value of 1.4. But this function was developed for use with mixing length approach, and is not adapted with transport equation turbulence models.

Transition criteria are then used to determine the transition location. Let us first recall the main factors impacting laminar-turbulent transition: pressure gradient, compressibility and perturbation level. Compressibility is not a main issue in this class of problems, except in case of turbine blades. Perturbation levels are either low (natural transition) or large (internal flows) and must be quantified. Pressure gradients may be characterized using the Pohlhausen parameter:

$$\Lambda_2 = \frac{\theta^2}{\upsilon}\frac{dU_e}{ds} \tag{1}$$

where θ is the momentum thickness of the boundary layer, υ the kinematic viscosity, s the chordwise coordinate and U_e the velocity modulus at the outer edge of the boundary layer. The AHD criterion (Arnal-Habiballah-Delcourt) [27] was derived from N-factor curves computed for Falkner Skan self similar attached velocity profiles. These curves are expressed as

$$N = N(Re_\theta - Re_{\theta_{cr}}, \Lambda_2) \tag{2}$$

where $Re_{\theta_{cr}}$ is the critical Reynold number at location s_{cr}, where the first instabilities start to grow. The use of the Mack's relationship ($N_T = -2.4\ \ln(Tu) - 8.43$) allows to express the transition Reynolds number Re_{θ_T} as a function of the external turbulence level Tu and the pressure gradient. The final criterion is based on the averaged Pohlhausen parameter, this average being computed from the critical point to the current one.

$$\overline{\Lambda_2} = \frac{1}{s-s_{cr}}\int_{s_{cr}}^{s}\frac{dU_e}{ds}ds \tag{3}$$

The criterion itself writes:

$$Re_{\theta_T} - Re_{\theta_{cr}} = -206\exp(25.7\overline{\Lambda_{2T}})[\ln(16.8Tu) - 2.77\overline{\Lambda_{2T}}] \tag{4}$$

It is activated after the detection of the critical location, identified by $Re_\theta = Re_{\theta_{cr}}$, where $Re_{\theta_{cr}} = \exp(\frac{52}{Hi} - 14.8)$, where $Hi = {\delta_1}/{\theta}$ is the incompressible shape factor of the boundary layer, estimated in elsA as a function of Λ_2 or $\overline{\Lambda_2}$. The formulation given here was developed for incompressible flow. In case of flow separation, a second criterion, due to Gleyzes [6], may be applied. It is a non local criterion, based on stability calculations for incompressible 2D detached self similar velocity profiles.

It was combined with AHD, thanks to J. Cliquet [28] in order to cover the full range of pressure gradients. To do this, a limit value of the incompressible shape factor $Hi(\overline{\Lambda_2})$, noted Hi_{switch} is defined, equal to 2.8 in Cliquet's thesis, below which AHD remains active. If *Hi* becomes larger than the limit, the Gleyzes criterion is used from that point on, with

$$N(s) = N_{switch} + \int_{Re_{\theta_{switch}}}^{Re_\theta} -\frac{2.4}{B}dRe_\theta \tag{5}$$

and

$$B = \begin{cases} \frac{-162.11093}{Hi^{1.1}} & if\ Hi > 3.36 \\ -73\exp((-1.56486(Hi - 3.02)) & if\ 2.8 < Hi < 3.36 \end{cases}$$

(6)

where N_{switch} represents the amplification reached at the point where $Hi = Hi_{switch}$. N_{switch} is obtained by inverting the AHD criterion expression :

$$N_{switch} = -8.43 - 2.4\ln\left[\frac{1}{16.8}\exp\left(2.77\overline{\Lambda_2} - \frac{Re_\theta - Re_{\theta_{cr}}}{206\exp(25.7\overline{\Lambda_2})}\right)\right] \quad (7)$$

The value of the transition N-factor N_T is again determined using Mack's relationship.

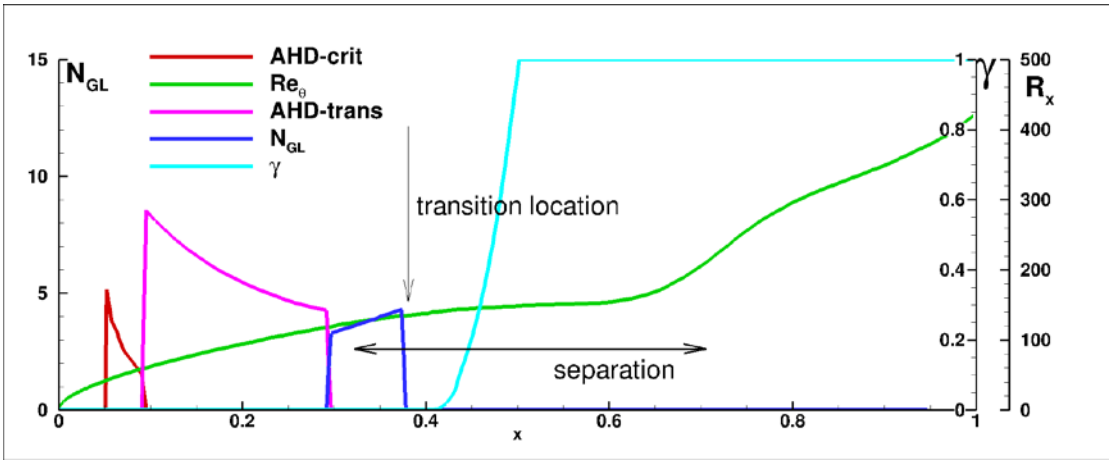

Figure 10.1 : Analysis of the modified AHD-GL criterion activation, SD7003 at 3° incidence

Several limitations may be stressed: relation 6 was determined for an incompressible flow and there is no provision to revert to AHD if transition does not occur within the separation. The AHD-GL criterion available in elsA [28] was revisited regarding the switching condition from AHD to GL, with the effect of allowing the prediction of both short and long bubbles. In order to improve the criterion, it was decided to increase Hi_{switch} to Hi_{switch}.= 3. + .145M_e so that the switch occurs closer to the separation point. A graphic analysis is proposed in Figure 10.1: The critical location is given by the crossing of curves Re_θ and AHD-crit, then the classical AHD criterion (AHD-trans) is activated up to the switching location (delayed from the initial version). Past this point, an N-factor curve is given by the GL criterion, down to the transition N-factor point. Note that the switch to GL still occurs upstream of the separation point, and that transition occurs downstream of separation. The original AHD criterion was also revisited to include the effects of compressibility and wall temperature [29].

This correction has two main benefits, first it avoids activating GL in cases where Hi may peak at 2.8 without any separation, and second it moves the transition point upstream of its original location, with improved results to be presented later. Another issue comes from the estimation of the shape factor, which in elsA is usually deduced from the value of the Pohlhausen parameter. With a well adapted mesh and selection of a precise numerical scheme, the shape factor directly computed from the incompressible integral thicknesses δ_1 and θ may also be used (but requires a specific setting of Hi_{switch}.). Test showed almost no difference from the result of fig. 10.1.

Next point of some importance, a distance is needed from the location where transition is predicted to where turbulence production is activated, in order to allow for both upstream and downstream move of the transition point during the iterating process and avoid a possible impact of transition on the upstream laminar boundary layer. In case of laminar separation, this proves difficult to manage as the evolution is rapid. Also, using a step function for the intermittency was observed to cause oscillations in the flow. So a continuously

rising function is preferred, and in elsA a parabolic rise of the intermittency function is proposed, with the intermittency reaching one when $Re_\theta = 1.15 Re_{\theta_T}$. This function is plotted in fig. 10.1 in light blue.

3.2 The LSTT Model

Following the DNS simulation of a laminar separation bubble under an imposed pressure gradient over a flat plate, derived from the OA209 pressure distribution, the evolution of turbulent quantities are obtained in the entire field. The starting idea in this section is to use this information in order to calibrate transition (or intermittency) functions allowing to reproduce the DNS evolution, while using classical k − ω turbulence models. It is assumed that the laminar extent of the bubble, from separation to transition, may be used as a characteristic length scale of the transition process, and that the intermittency functions may be expressed without any wall distance dependence. The analysis of the behaviour of k−ω turbulence models [30] showed that each model requires its own calibration.

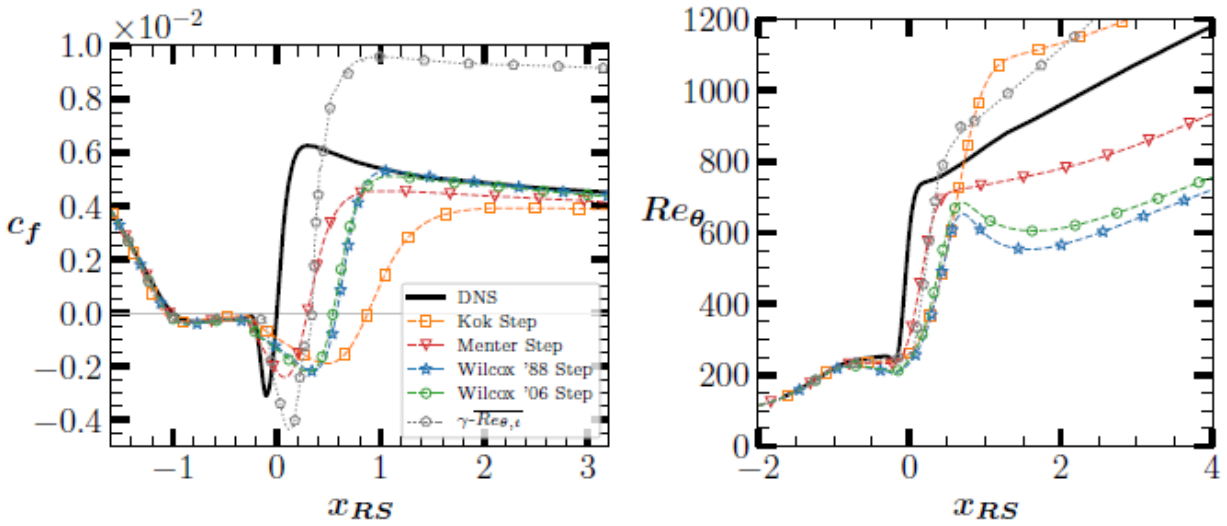

Figure 10.2 : Results obtained with a step function, imposed transition location and several turbulence models

Without any transition function, fig. 10.2 shows computed skin friction coefficient and momentum Reynolds numbers obtained with a number of two equations turbulence models, with imposed transition location and a step function in term on intermittency, compared to the DNS evolution. It is systematically visible that transition is delayed and requires a larger distance to reach full turbulence, compared to the DNS evolution. A family of functions was built with the objective to compensate the delays observed in fig. 10.2 and minimize the differences between the DNS and the RANS results. This recently developed transition modelling formulation, detailed in [31], intends to account for the turbulence growth in the separation bubble and in the downstream relaxation flow region. The Laminar Separation Transition Triggering (LSTT) functions are progressive in the streamwise direction, from the criteria-determined transition onset to full turbulence. They control both the production and destruction of turbulent quantities and are calibrated to obtain the best possible agreement with available DNS data [33]. The same turbulence models, each used with its own adapted transition function, produce the results in fig. 10.3: the dashed curves give the initial result, the full lines with symbols the corresponding one obtained with LSTT. A great improvement is visible.

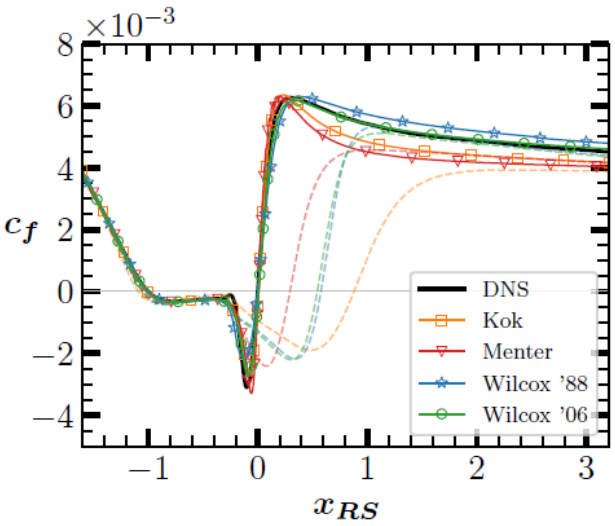

Figure 10.3 : Impact of the tailored transition function with computed transition : dashed curves without correction, symbols with the transitions function

Still for the flat plate case, fig. 10.4 shows the scaled turbulent Reynolds shear stress intensities obtained with the DNS (a), the LSTT model (b) with a Wilcox 2006 k − ω, and two results obtained with the Wilcox k − ω and imposed transition location, one with the stress limiter active (c) and the next without the stress limiter (d) in the bubble region, illustrating the strong undesired effect of the limiter in this case. Blocking the limiter over a defined space is a part of the LSTT model. Figures 10.4 (a) and (b) show large levels of turbulent shear stress past reattachment, related to an increased production of turbulence in this region, and show again a very good agreement between DNS and RANS-LSTT. Without the boost in production, reattachment is delayed as visible in figs. 10.4 (c) and (d). This model has been applied to the SD7003 configuration (presented in the last section) as well as a number of other cases [31][33], proving to be quite effective, and not limited to its initial configuration.

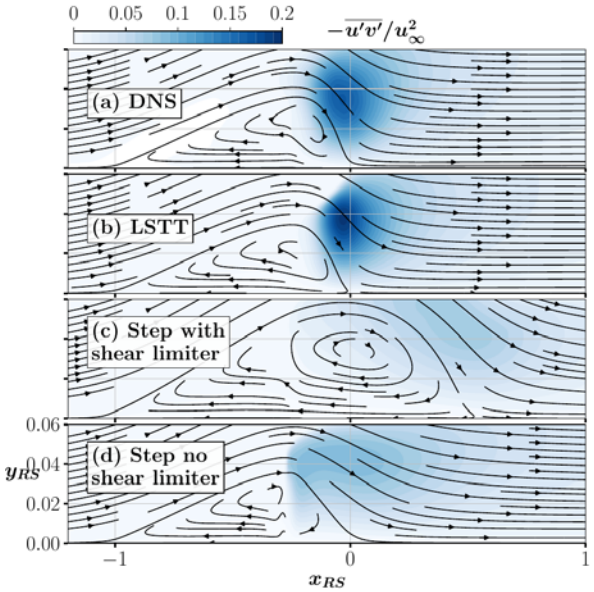

Figure 4: Maps of Reynolds stress intensities from DNS and LSTT, compared to unforced evolutions

3.3 Menter-Langtry $\gamma - \overline{R_{\theta_T}}$ Approach

The approach proposed by Menter & Langtry [34][35][36], based on two transport equations for an intermittency γ and a transition Reynolds number $\overline{R_{\theta_T}}$ is also available in elsA, using closures developed by C. Content [37] and A. Minot [19] (the later specifically developed to consider detached flows over turbine blades). While the transition criterion contained in this approach is rather crude, the ease of application and the fairly good results which may be obtained on turbine blades [38] have made this approach a popular one, at least for that class of applications.

This model is based on two transport equations, one for an intermittency function γ and one for a Reynolds number $\overline{R_{\theta_T}}$.

$$\frac{\partial \rho \gamma}{\partial t} + \frac{\partial \rho U_j \gamma}{\partial x_j} = P_\gamma - E_\gamma + \frac{\partial}{\partial x_j}\left[\left(\mu + \frac{\mu_t}{\sigma_f}\right)\frac{\partial \gamma}{\partial x_j}\right] \tag{8}$$

$$\frac{\partial \rho \overline{R_{\theta_T}}}{\partial t} + \frac{\partial \rho U_j \overline{R_{\theta_T}}}{\partial x_j} = P_{\theta_T} + \frac{\partial}{\partial x_j}\left[\sigma_{\theta_T}(\mu + \mu_t)\frac{\partial \overline{R_{\theta_T}}}{\partial x_j}\right] \tag{9}$$

Note that γ here is not the physical intermittency, but becomes a field controlling the laminar or turbulent nature of the boundary layer, while $\overline{R_{\theta_T}}$ is linked to a transition criterion. $\overline{R_{\theta_T}}$ is initialized using the Langtry's transition correlation outside the boundary layer, function of the local turbulence level and of the pressure gradient, and then advected inside the boundary layer. The production term in the γ equation is activated when the local value of Re_θ becomes larger than $\overline{R_{\theta_T}}$. The production term in the turbulence model is then multiplied by γ, controlling the turbulent kinetic energy rise from the model. P_γ represents the intermittency production term, defined as

$$P_\gamma = F_{length} c_{a1} \rho S (\gamma F_{onset})^{0.5} (1 - c_{e1}\gamma)$$

where two functions, F_{onset} and F_{length} control the activity and the amplitude of the production.

F_{onset} is related to a ratio $\frac{Re_v}{2.193 Re_{\theta_c}}$, where $Re_v = \frac{\rho y^2 \Omega}{\mu}$ represents the local vorticity Reynolds number introduced by van Driest and Blumer [39] for the laminar boundary layer. $\frac{\max(Re_v)}{2.193}$ provides a local estimate for Re_θ. Production is set to zero when the ratio remains below one. F_{length} controls the rate of production and thus the length of the transition region. Both Re_{θ_c} and F_{length} functions are expressed as functions of $\overline{R_{\theta_T}}$.

In case of laminar separation, an increase of the γ values is imposed if the local value of the ratio $\frac{Re_v}{3.235 Re_{\theta_c}}$ becomes larger than one, hence after a further increase of Re_v downstream of transition, in order to increase the turbulent kinetic energy production some distance downstream of transition. In this case, there is no modification of the transition criterion in relation to the presence of separation, but only an acceleration of turbulence production downstream of the transition location.

4.0 COMPARISON OF THE THREE METHODS

In a first part of the work, there is no specific intermittency function used to control the transition region and the rise in turbulent kinetic energy k. Instead, a predetermined level of kinetic energy is imposed, in a manner here decoupled from the turbulence level used for transition triggering. The method proposed by Spalart and Rumsey is used, imposing at the upstream boundary the desired levels in k and ω and blocking further decay with cut-off factors set to one. The objective of this setting is to accelerate the rise of

turbulence past transition, since preliminary computations showed a visible impact. In the presented results, $(\rho k)_{amb}$ is non dimensionalised with $(\rho U^2)_{ref}$ so the values used in fig. 10.5 correspond to a turbulence level

(for the turbulence model) of 1%. The turbulence level for transition Tu_{ext} is fixed and given in the figure.

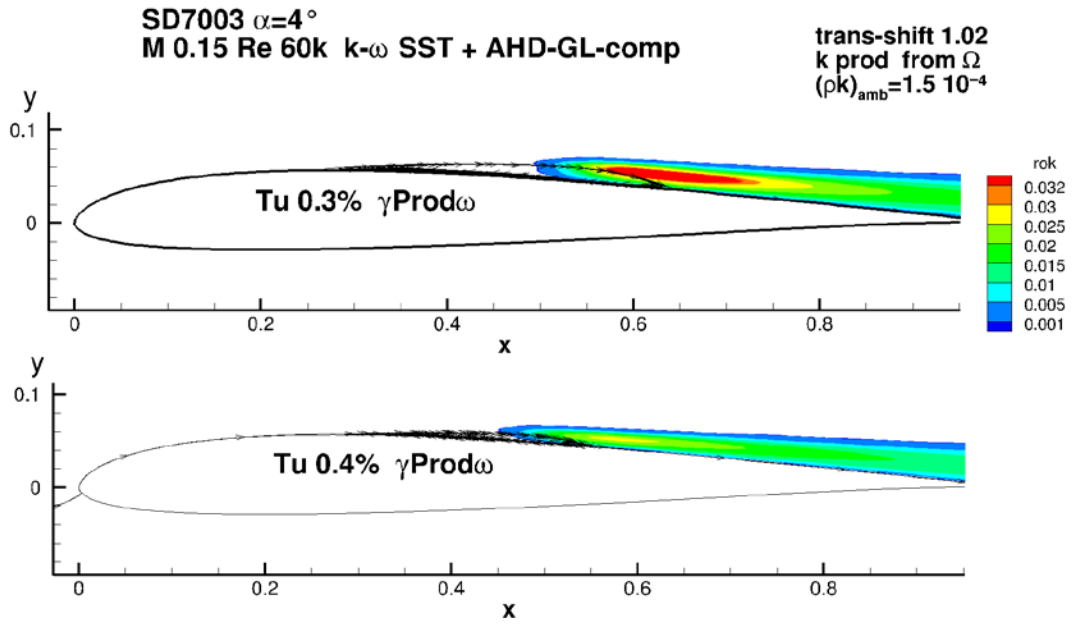

Figure 10.5 : SD7003 results at 4° incidence : maps of turbulent kinetic energy level

Results in figure 10.5 were obtained with the SD7003 profile at Re_C = 60000 and 4° incidence, showing the evolution of the separation zone for several values of the turbulence parameter. In this case, a short distance is imposed between the transition location and the activation of the turbulence model in order to avoid a coupling between the transition region and the criterion. The consequence is that the calculated transition location needs to be moved a short distance upstream, and that is obtained with an increase of the imposed turbulence level, here 0.3%. With this method, the largest predicted steady separation at Tu = 0.3% should be similar to a LES result computed with very low turbulence level.

In addition, the k production term should be expressed as a function of the vorticity tensor Ω_{ij} instead of the shear stress S_{ij}, and the dissipation production *Prod(ω)* is also scaled by the intermittency to avoid large values of the dissipation ω in the laminar region.

With these settings, comparisons to the LES results of [13] are shown in figures 10.6. Separation and re-attachment points are in good agreement. The friction coefficient peak is quite well reproduced in the downstream, transitional part of the bubble. A larger discrepancy remains past the reattachment point, which may be due to the absence of a specific intermittency function accelerating the turbulence production.

Similar results were obtained with the ONERA-D profile, and compared to measurements of pressure distribution, see figures 10.7 and 10.8. Results seem more satisfactory at this higher Reynolds number and in case of a short bubble.

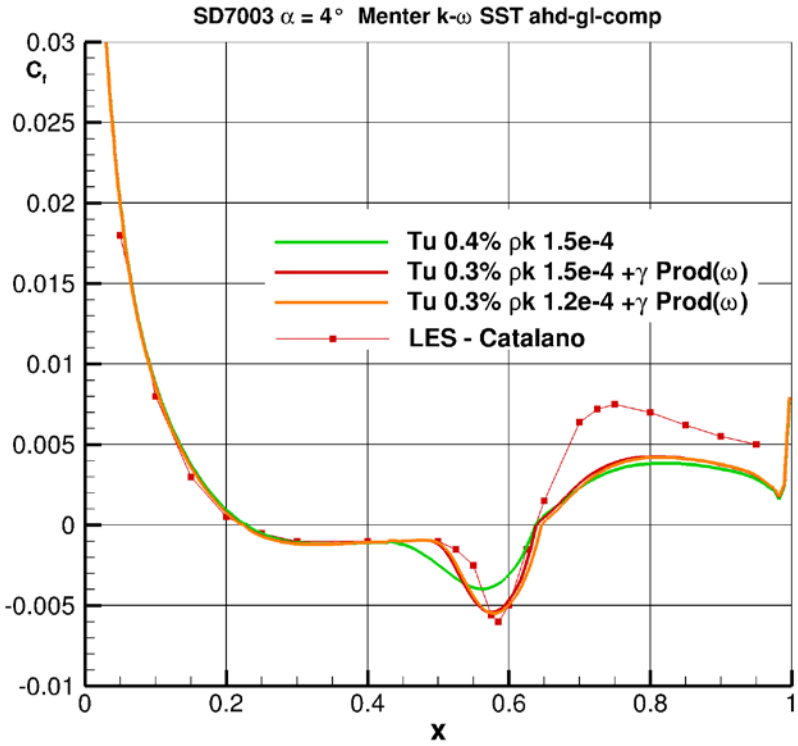

Figure 10.6 : Comparison of frictions coefficients obtained with AHD-GL and with LES [13]

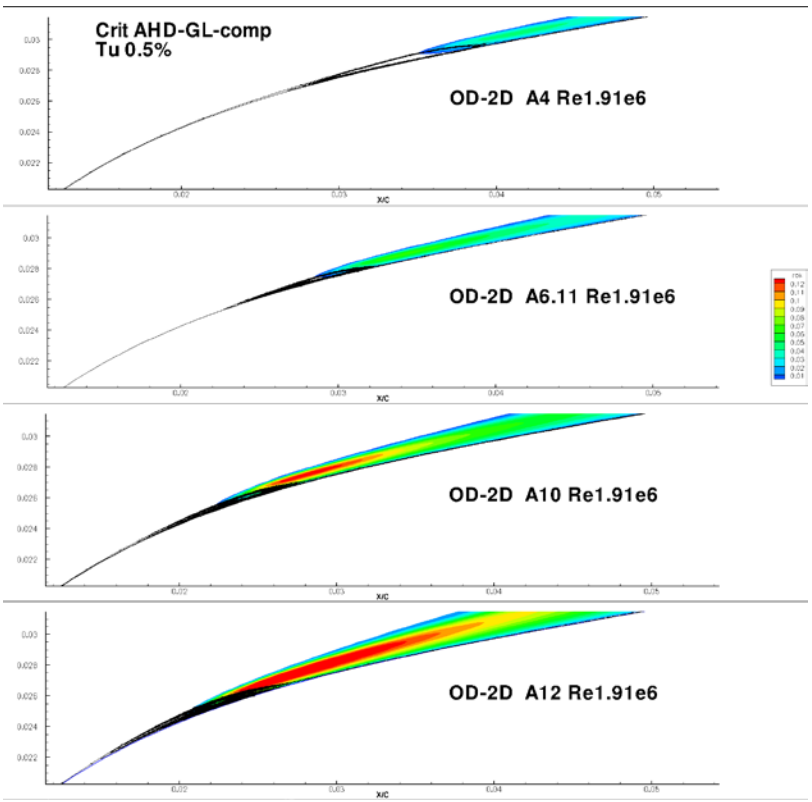

Figure 10.7 : Short bubble prediction for ONERA-D profile at several incidences – Maps of turbulent kinetic energy levels. Incicences 4°, 6.11°, 10° and 12° from top to bottom

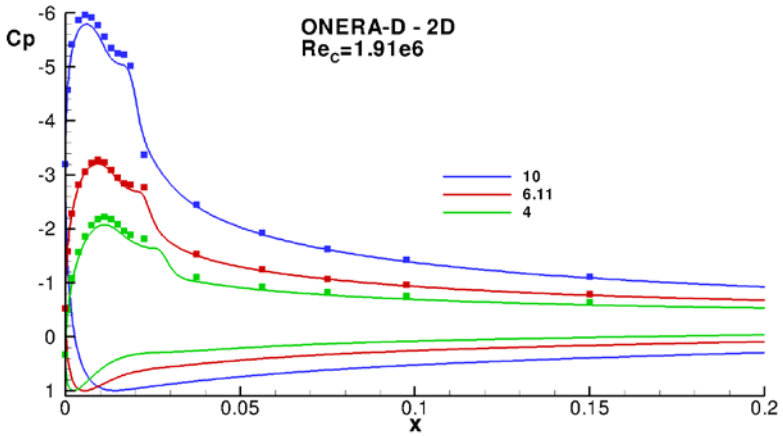

Figure 10.8 : Predicted pressure distributions (lines) compared to experiments (symbols)

The presented tools and results so far show that the modified GL criterion allows considering both short and long bubbles and gives a physically correct response to a change in transition location, or turbulence level. Questions remain regarding the calibration of the method, the distance required to reach full turbulence production, and the level of ambient kinetic energy. Most important, fig. 10.6 shows that the relaxation region, past re-attachment, is poorly reproduced, which probably comes from a deficit in turbulence production in this region as was observed in fig. 10.4.

Applying the LSTT model on the SD7003 at the same incidence produces results plotted in fig. 10.9, showing a much better agreement with the LES results in the relaxation region, past reattachment. This result has been obtained with the AHD-GL criterion together with the specific LSTT 'intermittency' function and a de-activation of the SST limiter over a given distance, in order to correctly accelerate the production of turbulence past the transition point. In the same figure, two results obtained with the $\gamma - \overline{R_{\theta_T}}$ method are also plotted, using two correlations available in elsA, a general use CH10 and a specifically optimized one for turbines blades, MMP16V2, due to A. Minot [19]. While the transition location is quite well captured in the four cases, the C_f peak amplitude is correctly reproduced using the classical criterion but becomes too wide when using the $\gamma - \overline{R_{\theta_T}}$ method. In the relaxation region, the worst results are obtained with the $\gamma - \overline{R_{\theta_T}}$ method, showing that the corrective term for separation γ_{sep}, which may rise up to two, fails to improve significantly the predictions.

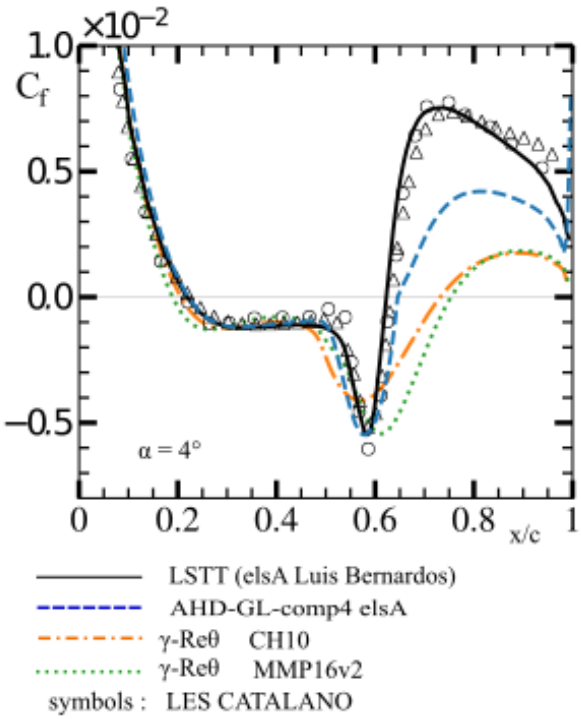

Figure10. 9 : SD7003 results at 4 o incidence, comparing $\gamma - \overline{R_{\theta_T}}$ and AHD-GL with a tailored 'intermittency' function to the LES reference (symbols)

Figure 10.10 provides comparisons between the criterion approach and the $\gamma - \overline{R_{\theta_T}}$ method for the T106C turbine blade at two values of the Reynolds number and a turbulence level of 1.8%. This turbine blade was selected for the creation of Minot's correlations [14]. The two methods are seen to give a good agreement with measurements at the largest Reynolds number (fig. 10.10b), while transition criterion method does not allow to capture the separation region at the lowest Reynolds number (fig. 10.10a). This is not surprising, the criterion approach being by definition restricted to low turbulence conditions, with $Tu_{max} \approx 1\%$. When looking at larger values of turbulence levels, better results are almost systematically obtained, at least for turbine blades, with the $\gamma - \overline{R_{\theta_T}}$ method.

A second comparison, in case of the T106C turbine blade, is given in fig. 10.11, comparing LSTT with $\gamma - \overline{R_{\theta_T}}$ at an intermediate Reynolds number of 120 000. While $\gamma - \overline{R_{\theta_T}}$ agrees well with the measurements, the LSTT model with a transition N-factor of 2.9 (corresponding to the given Tu value) does not correctly capture the separation. Increasing the transition N-factor to 10 improves significantly the comparison. Looking at the solution, it appears that transition is predicted almost at the separation point, much too early, with $N_T = 2.9$. The actual turbulence level at the frontier of the boundary layer in the vicinity of the separation point and transition onset may in fact be lower than the given value. Another point is that Mack's law was proposed for 2D transition resulting from Tollmien Schlichting waves, and may not be adapted in case of Kelvin-Helmholtz instabilities. A calibration effort might become necessary in order to allow the method to consider different types of instabilities.

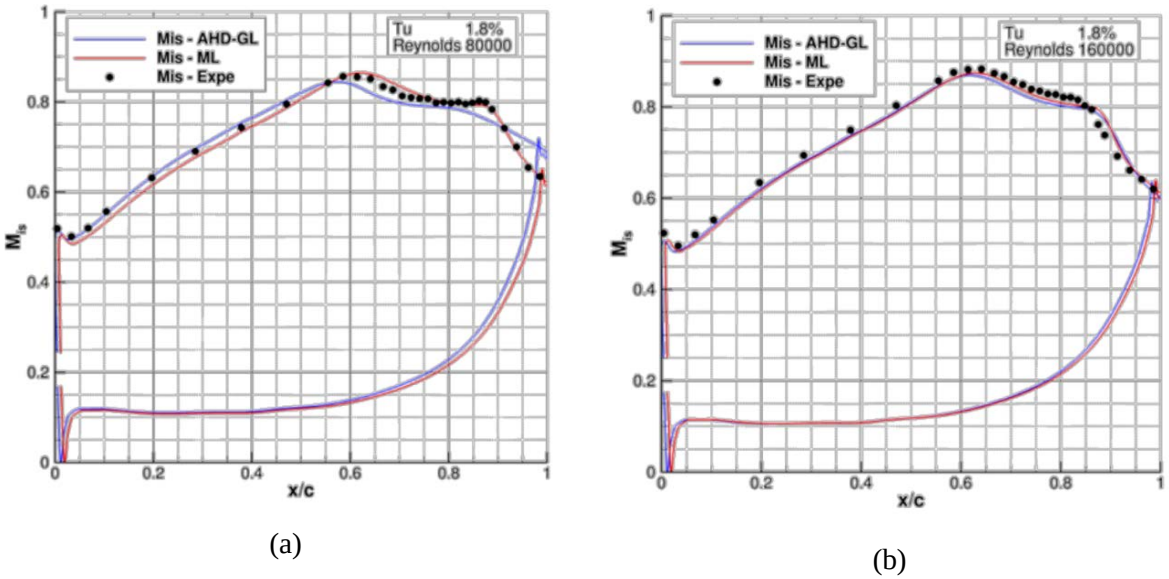

(a) (b)

Figure 10.10 : Results obtained for the T106C turbine blade
(blue lines: transition criterion approach, red lines: $\gamma - \overline{R_{\theta_T}}$ approach, symbols: experiments)

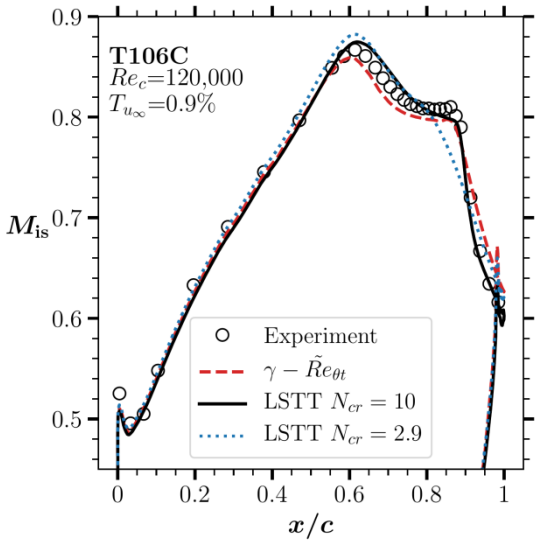

Figure 10.11 : T106C result at Re 120000 (LSTT & $\gamma - \overline{R_{\theta_T}}$)

In order to test the MMP16V2 correlation at low turbulence levels on a very different configuration, the $\gamma - \overline{R_{\theta_T}}$ method was applied to a SD7003 configuration at 8 deg. incidence. Results in fig. 10.12 show that almost the same solution may be obtained with quite different turbulence settings. The first two results were obtained with a doubling of the imposed Tu_e values for the transition criterion, and the third is computing Tu from the local k values, with an estimated value of 0.25% (not constant around the profile). The expected impact of a change of transition location is not visible in this case characterized by very small value of freestream turbulent intensity. In this configuration, the transition location has strong impact on the flow topology and must be correctly predicted. The $\gamma - \overline{R_{\theta_T}}$ method proves not to be robust enough for this kind

of computation.

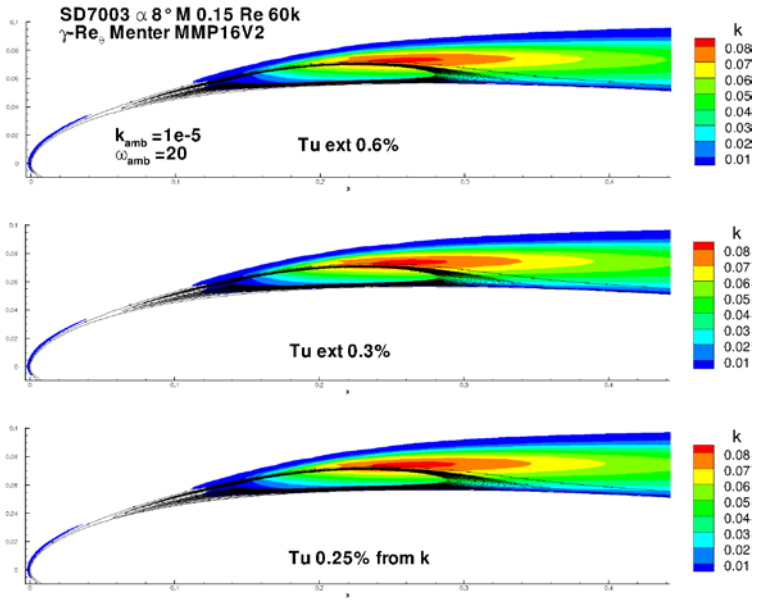

Figure 10.12 : Bubble prediction using the Menter method at low turbulence level

In turbomachinery applications, the interaction between wakes and profiles are quite often encountered. This leads to the phenomenon of calming. Firstly, far from the incoming wakes, a laminar separation bubble is observed. Then, when the wake impinges the boundary layer, transition onset is located upstream, often before the separation point. The laminar separation bubble is then suppressed. Once the wake is downstream, the residual fluctuations leads to a laminar boundary layer with a shape factor lower than 2.59. Thus this perturbed laminar boundary layer is able to resist to strong adverse pressure gradient and the separation point is observed downstream of the initial position. The laminar bubble is observed but with smaller length and thickness. Finally, when the incoming wakes are far from the transitional boundary layer, the nominal laminar separation bubble is recovered. The time-averaged flow predicted by Menter-Langtry model is in good agreement with experimental data in terms of isentropic Mach number distribution over the airfoil, as shown in figure 10.13a. Figure 10.13b depicts the skin friction modulus along the chord and two wake passing periods. The black lines correspond to the separation (upstream line) and reattachment points (downstream line). The grey dashed line is relative to these points without incoming wakes. In that case, without the wakes, there is no reattachment before the trailing edge, as experimentally observed. The high value of friction is linked to the trajectory of the incoming wakes. The calming phenomenon is well captured by simulations as the laminar separation bubble is reduced when the incoming wake impinges the boundary layer close to the transition area. At higher Reynolds number or higher freestream turbulent intensity, the bubble may even be suppressed by the interaction with the wake.

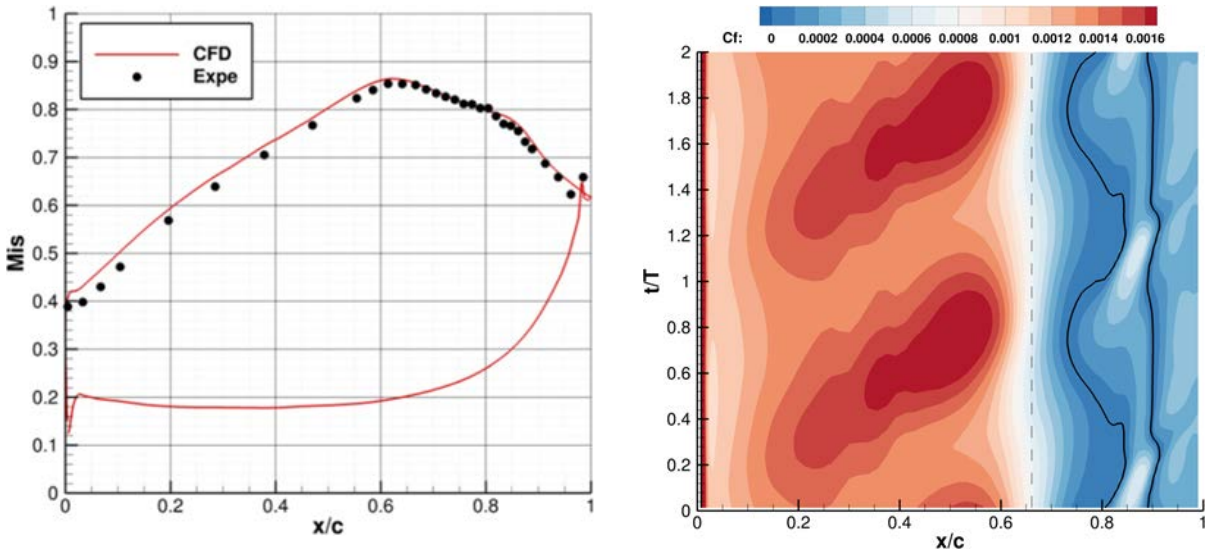

(a) (b)

Figure 10.13 : Calming effect prediction over T106C turbine airfoil. Re_{2is} = 160 000 and Tu_∞ = 0.9%

5.0 CONCLUSION

The corrected AHD-GL criterion has been shown to allow the prediction of laminar-turbulent transition occurring inside a laminar bubble in low turbulence, low Reynolds number configurations. The same model also allows to compute larger Reynolds number cases with short bubbles. The initial part of the transition region, with the minimum C_f region, is well captured while the relaxation zone, past re-attachment, is not so well reproduced.

The methods of prescribing an imposed value of $(\rho k)_{amb}$ seem to lack robustness, small variations in $(\rho k)_{amb}$ may impact the convergence process.

A well tailored boost of turbulent kinetic energy production is required to account for the rise of turbulence, and has to be specifically determined for each turbulence model. Also, the shear stress limiter (SST) must be de-activated over a determined region past the transition point. Both transition location (from the criterion) and the production boost need to be specified with a good precision for low turbulence cases.

In low turbulence flows, these methods are generally more precise than the Menter & Langtry approach. Furthermore, the γ_{sep} correction in Menter & Langtry, introduced to generate a boost of production in the region of separation, fails to do so in the relaxation region in case of the SD7003.

On the other hand, the Menter & Langtry approach does not require the computation of boundary layer quantities and is better adapted to recent massively parallel computations, but with a lesser quality of physical modelling. For highly turbulent flows, the Menter & Langtry formulation is at present the most accurate model, especially for turbine applications. The transition location does not need to be as precisely determined as for low turbulence cases. This approach has been demonstrated here in a complex test case involving periodic wake impingement on a turbine blade, leading to the calming effect, in which the wake results in a more stable laminar boundary layer in a part of the cycle with a reduction in the size of the separation region.

The laminar kinetic energy models currently under development should improve in a near future the quality of predictions in large turbulence flows.

These recently developed modelling tools are now being tested in various configurations, illustrated by a first set of test cases in the present paper. More work is needed to consider applying these tools to realistic swept wings, helicopter rotors and complex flow configurations is. The specific case of laminar transonic wings presenting a shock induced trailing edge separation may be computed in a range of conditions, but RANS fails to correctly predict cases with open separation. Also, high lift configurations presenting small leading edge separations need to see these separation bubbles correctly predicted in order to ensure a precise evaluation of performance. Extending the current work towards transonic applications is our next goal. Modelling activities will continue with a GARTEUR project, AG59, which started in 2019.

AKNOWLEDGEMENTS

Work presented here is mostly the product of an internal ONERA project, called PR BUDLETIN, allowing fruitful cooperation from several groups in the 'Office'. Thanks are due to F. Richez and V. Gleize, from ONERA, both very involved in this topic.

REFERENCES

[1] M. Drela, "XFOIL: An analysis and design system for low Reynolds number airfoils", in T.J. Mueller "Low Reynolds number aerodynamics", Lecture Notes in Engineering, vol. 54, Springer Verlag, 1989

[2] C. Laurent, "Etude d'écoulements transitionnels et hors équilibre par des approches DNS et RANS", PhD Thesis, ParisTech, Ecole Nationale Supérieure d'Arts et Métiers, déc. 2012

[3] M. Galbraith and M. Visbal, "Implicit large eddy simulation of low Reynolds number flow past the SD7003 airfoil", AIAA Paper 2008-225, Reno, Nev.,Jan. 2008

[4] P. Catalano and R. Tognaccini, "Turbulence modeling for low-Reynolds-number flows", AIAA Journal, vol. 48, no. 8, pp. 1673–1685, 2010.

[5] S. Roberts and M. Yara, "Modeling transition in separated and attached boundary layers", ASME Journal of Turbomachinery, vol. 127, pp. 402–411, Apr. 2005

[6] C. Gleyzes, J. Cousteix, and J. Bonnet, "Theoretical and experimental study of low Reynolds number transitional separation bubbles", Proceeding of the conference on low Reynolds number airfoil aerodynamics, UNDAS-CP-77B123, University of Notre Dame, Indiana, Jun. 1985

[7] P. Dini, M. Selig, and M. M.D., "Simplified linear stability transition prediction method for separated boundary layers", AIAA Journal, vol. 30, no. 8, pp. 1953–1961, Aug. 1992

[8] J. Windte, U. Scholz, and R. Radespiel, "Validation of the RANS-simulation of laminar separation bubbles on airfoils", Aerospace Science and Technology, vol. 10, pp. 484–494, 2006.

[9] R. Radespiel, J. Windte, and U. Scholz, "Numerical and experimental flow analysis of moving airfoils with laminar separation bubbles", AIAA Journal, vol. 45, no. 6, pp. 1346–1356, 2007.

[10] F. Richez, V. Gleize, I. Mary, and C. Basdevant, "Simulation and modeling of a laminar separation bubble on airfoils", IUTAM symposium on Unsteady Separated Flows and their Control, Corfu, Greece, Jun. 2007

[11] R. Arina, C. Atkin, E. Hanff, K. Jones, T. Lekas, M. Ol, M. Khalid, B. McAuliffe, J. Paquet, M. Platzer, R. Radespiel, U. Rist, J. Windte, and W. Yuan, "AVT-101 Final Report: Experimental and computational investigations in low Reynolds number aerodynamics, with applications to micro air vehicles", RTO Tech. Rep., 2006

[12] O. Marxen, M. Lang, U. Rist, and S. Wagner, "A combined experimental/numerical study of unsteady phenomena in a laminar separation bubble", Flow, Turbulence and Combustion, vol. 71, no. 1-4, pp. 133–146, 2003

[13] P. Catalano and R. Tognaccini, "Influence of free-stream turbulence on simulations of laminar separation bubbles", AIAA Paper 2009-1471, Orlando, Fl., Jan. 2009

[14] A. Minot, X de Saint Victor, J. Marty, and J. Perraud, "Advanced numerical setup for separation induced transition on high lift turbine flows using the Langtry and Menter model", in ASME Turbo Expo, ASME, Montreal, Canada, 2015

[15] J. Perraud, H. Deniau, and G. Casalis, "Overview of transition prediction tools in the elsa software", in ECCM ECFD VI, ECCOMAS, Barcelona, Spain, 2014.

[16] L. Jecker, O. Vermeersch, H. Deniau, G. Casalis, and E. Croner, "A new laminar kinetic energy model for RANS simulations of bypass transition", AIAA Paper 2017-3457, Denver, Col., Jun. 2017

[17] M. Kruse and R. Radespiel, "Measurement of a laminar separation bubble on a swept horizontal tailplane using μ-PIV", AIAA Paper 2008-4054, Seattle, Wash., Jun. 2008

[18] P. R. Spalart and C. L. Rumsey, "Effective inflow conditions for turbulence models in aerodynamic calculations", AIAA journal, vol. 45, no. 10, pp. 2544–2553, 2007

[19] A. Minot, "Modélisation de la transition laminaire-turbulent par rugosité et bulbe de décollement laminaire sur les aubes de turbomachines", PhD thesis, Université de Toulouse, ISAE-SUPAERO, May 2016

[20] K. Richter, A. Le Pape, T. Knopp, M. Costes, V. Gleize, and A. Gardner, "Improved two-dimensional dynamic stall prediction with structured and hybrid numerical methods", Journal of the American Helicopter Society, vol. 56, no. 4, Oct. 2011

[21] F. Richez, I. Mary, V. Gleize, and C. Basdevant, "Near stall simulation of the flow around an airfoil using zonal RANS/LES coupling method", Computers & Fluids, vol. 37, no. 7, pp. 857–866, 2008

[22] J. Donovan and M. Selig, "Low Reynolds number airfoil design and wind tunnel testing at Princeton University", in Low Reynolds number aerodynamics, vol. 54, Springer, 1989, pp. 39–57

[23] D. Olson, A. Katz, A. Naguib, D. Koochesfahani M.M.and Rizetta, and M. Visbal, "An investigation of the effect of freestream turbulence on the laminar separation bubble on an SD7003 airfoil", Paper 2011-395, Orlando, Fl., Jan 2011

[24] P. Catalano and R. Tognaccini, "Rans analysis of the low-Reynolds number flow around the SD7003 airfoil", Aerospace Science and Technology, vol. 15, pp. 615–626, 2011

[25] J. Michalek, M. Monaldi, and T. Arts, "Aerodynamic performance of a very high lift low pressure turbine airfoil (T106C) at low reynolds and high mach number with effect of free stream turbulence

intensity", Journal of Turbomachinery, vol. 134, no. 6, 2012

[26] D. Arnal, "Transition prediction in transonic flow", in Transsonicum III, IUTAM Symposium, Gottingen, Germany. Springer-Verlag, 1988

[27] D. Arnal, H. Habiballah, and E. Coustols, "Théorie de l'instabilité laminaire et critères de transition en écoulement bi et tridimensionnel", La Recherche Aérospatiale, vol. 1984-2, 1984

[28] J. Cliquet, R. Houdeville, and D. Arnal, "Application of laminar-turbulent transition criteria in Navier-Stokes computations", AIAA Journal, vol. 46, no. 5, pp. 1182–1190, 2008

[29] J. Perraud and A. Durant, "Stability-based Mach zero to four longitudinal transition prediction criterion", Journal of Spacecrafts and Rockets, vol. 53, no. 4, pp. 730–742, 2016

[30] L. F. Bernardos, F. Richez, V. Gleize, and G. Gerolymos, "On the k-ω models behavior in the boundary-layer downstream of a short transitional separation bubble", AIAA Paper 2018-376, Kissimee, Fl., Jan. 2018

[31] L. Bernardos, F. Richez, V. Gleize, and G. A. Gerolymos, "Algebraic nonlocal transition modeling of laminar separation bubbles using k-ω turbulence models", AIAA Journal, vol. 57, no. 2, pp. 553–565, 2019.

[32] C. Laurent, I. Mary, V. Gleize, A. Lerat, and D. Arnal, "DNS database of a transitional separation bubble on a flat plate and application to RANS modeling validation", Computers and Fluids, vol. 61, pp. 21–30, 2012.

[33] L. Bernardos, F. Richez, and V. Gleize, "RANS modeling of laminar separation bubbles around airfoils at low Reynolds conditions", AIAA Paper 2019-2922, Dallas, Texas, Jan 2019

[34] F. R. Menter, T. Esch, and S. Kubacki, "Transition modelling based on local variables", in ETMM 5, 5th International Symposium on Engineering Turbulence Modelling and Measurements, Mallorca,Spain, 2002

[35] F. R. Menter, R. B. Langtry, S. R. Likki, Y. B. Suzen, P. G. Huang, and S. Völker, "A correlation-based transition model using local variables Part I - model formulation", in ASME GT2004-53452, ASME Turbo Expo 2004 Power for Land, See and Air, Vienna, Austria, Jun. 2004

[36] R. B. Langtry, "A correlation-based transition model using local variables for unstructured parallelized CFD codes", PhD Thesis, Stuttgart University, May 2006.

[37] C. Content, "Méthode innovante pour le calcul de la transition laminaire-turbulent dans les codes Navier-Stockes", PhD Thesis, Institut Supérieur de l'Aéronautique et de l'Espace, May 2011

[38] A. Benyahia, "Mise en oeuvre et évaluation d'un modèle de transition à équations de transport pour la simulation d'écoulements en turbomachines", PhD Thesis, Université Toulouse III, Ecole Doctorale MEGEP, Dec. 2012

[39] E. R. van Driest and C. B. Blumer, "Boundary layer transition : Free-stream turbulence and pressure gradient effects", AIAA Journal, vol. 1, no. 6, pp. 1303–1306, 1963